Astronomy & Astrophysics manuscript no.
(will be inserted by hand later)

Low mass T Tauri and young brown dwarf candidates in the Chamaeleon II dark cloud found by DENIS

M.H. Vuong[1⋆], L. Cambrésy[2], and N. Epchtein[1]

[1] Observatoire de la Côte d'Azur, Département Fresnel, 06304 Nice Cedex, France; vuong@discovery.saclay.cea.fr, epchtein@obs-nice.fr
[2] California Institute of Technology, IPAC/JPL, CA 91109 Pasadena, USA; laurent@ipac.caltech.edu

Accepted 2001 September 5

Abstract. We define a sample designed to select low-mass T Tauri stars and young brown dwarfs using DENIS data in the Chamaeleon II molecular cloud. We use a star count method to construct an extinction map of the Chamaeleon II cloud. We select our low-mass T Tauri star and young brown dwarf candidates by their strong infrared color excess in the $I-J/J-K_s$ color-color dereddened diagram. We retain only objects with colors $I-J \geq 2$, and spatially distributed in groups around the cloud cores . This provides a sample of 70 stars of which 4 are previously known T Tauri stars. We have carefully checked the reliability of all these objects by visual inspection on the DENIS images. Thanks to the association of the optical I band to the infra-red J and K_s bands in DENIS, we can apply this selection method to all star formation regions observed in the Southern Hemisphere. We also identify six DENIS sources with X-ray sources detected by *ROSAT*. Assuming that they are reliable low-mass candidates and using the evolutionary models for low-mass stars, we estimate the age of these sources between 1 Myr and < 10 Myr.

Key words. ISM: clouds – ISM: dust, extinction – ISM: individual objects: Chamaeleon

1. Introduction

The Chamaeleon complex is one of the nearest star formation regions to the Sun (between 160 and 180 pc, Whittet et al., 1997). It consists of three main dark clouds, designated Chamaeleon (Cha) I, II and III (Schwartz, 1977). Its relative proximity, high Galactic latitude (b $\approx -17°$) and young age ($\sim 10^6$ yrs) make it an ideal location to search for low-mass T Tauri stars (TTS) and young brown dwarfs. The low-mass population can provide constraints on the shape of the initial mass function (by investigating the slope), which is still poorly determined at low masses (Tinney, 1993; Méra et al., 1996).

Young stellar objects are characterised by their Hα emission line (Hartigan, 1993) and an infrared excess that reveals the presence of circumstellar material in the near infrared (Larson et al., 1998; Oasa, Tamura, & Sugitani, 1999; Gómez & Kenyon, 2001), the mid-infrared (ISO, Persi et al., 2000) and the far-infrared (IRAS, Prusti et al., 1992). X-ray observations (ASCA, ROSAT) allow the identification of young stellar objects (Yamauchi et al., 1998; Alcalá et al., 2000). The origin of the X-ray emission from the low-mass pre-main sequence stars may be due to an enhanced dynamo activity with a coupled process of surface convection and differential rotation of a star or between a star and the inner disks (*e.g.* in ρ Oph, Montmerle et al., 2000). The millimeter observations such as the detection of the CO and CS lines that reveal the gas emission and the outflows often allow to characterise young stellar objects (Olmi et al., 1994).

Weak line TTS are known as pre-main sequence objects without a disk and are usually found to be associated with X-ray sources. In contrast, classical TTS with a circumstellar disk show strong Hα emission, and excess IR emission. Brown dwarfs are low-mass stars ($<$0.08 $M_\odot$) which never reach the reaction of hydrogen fusion. They are mainly powered by gravitational energy. Therefore they are relatively faint objects and can only be detected at nearby distances ($\lesssim$ 30 pc). However, young brown dwarfs are much more luminous ($\sim$100 times more than field brown dwarfs). Such young brown dwarfs can be found in star forming regions out to a few 100 pc (Neuhäuser & Comerón, 1999).

The Cha II has not been mined as thoroughly as the Cha I cloud. In the Chamaeleon clouds, the pre-main-sequence stars, mainly TTS, were first discovered by Schwartz (1977). No brown dwarfs have yet been found in

Send offprint requests to: Mỹ Hà Vuong
⋆ Present address: Service d'Astrophysique, CEA Saclay, 91191 Gif-sur-Yvette, France

the Cha II. Recently, Comerón et al. (2000) found eleven young brown dwarfs in the Cha I cloud from pointed IR observations. With the advent of large near-IR surveys (DENIS, 2MASS), it is now possible to easily identify such samples across large regions of the sky. Cambrésy et al. (1998) have used DENIS data to find young stellar objects in the Cha I cloud.

In this paper, we introduce a low-mass star sample in the Cha II dark cloud, extracted from the DENIS survey. Sect.2 describes the observations and the data reduction. In Sect.3, we construct an extinction map of the Cha II cloud, and present the color-color $I-J/J-K_s$ diagram used to search for new low-mass members. Finally, Sect.4 discusses the position of our sources on the color-magnitude diagram using the evolutionary tracks for low-mass stars as modeled by Baraffe et al. (1998).

2. DENIS Observations and data reduction

The observations presented in this paper have been obtained from the DEep Near Infrared Survey of the Southern Sky (DENIS, Epchtein et al., 1997) between 1996 March and 1998 May at La Silla using the ESO 1m telescope. They cover an area of $2.42^\circ \times 3.50^\circ$ centered at 13h 00m 00s in right ascension (J2000) and -76° $45'$ $00''$ in declination (J2000) in three bands $I(0.8\mu m)$, $J(1.25\mu m)$ and $K_s(2.15\mu m)$. Limiting magnitudes at 3σ are 18, 16 and 13.5 in I, J and K_s bands. It consists of 24 strips each containing 180 images of $12' \times 12'$ taken at constant right ascension along an arc of 30° in declination. There is a $2'$ overlap between each two adjacent images. For the adjacent strips, the overlap is also $2'$ for the image in the north. The overlap becomes more important when we move to the south by a simple projection effect (this is particularly important for the Chamaeleon complex because of its proximity to the South Pole).

The data reduction took place at the Paris Data Analysis Center (PDAC). The source extraction used PSF fitting. The astrometric calibration was obtained by cross-correlation with the USNO-PMM catalog (Monet et al., 1998). The absolute astrometry is then fixed by the accuracy of this catalog ($\sim 0.5''$ at 3σ, Deutsch, 1999). The internal accuracy of DENIS observations derived from the overlapping regions of adjacent images is $\sim 0.35''$ (3σ). For the determination of the photometric zero points, all standard stars observed during a given night were used. We have checked the photometric uncertainties of sources in the Cha II cloud by comparing the magnitudes of stars detected in more than one image. This yields photometric uncertainties of ~ 0.05, 0.12 and 0.15 for I, J and K_s, respectively. All point sources detected in an image are taken into account in the PDAC procedures. Consequently, an object can appear several times, when it is located in the overlapping regions. To eliminate these multiple detections, we first determine the radius in which two point sources are considered to be the same object. To determine this radius, we use the histogram of the position differences of sources in the overlapping regions between two adjacent images. The distribution drops to 0 identifications at a radius of $2''$ before starting to pick up unrelated stars beyond $10''$. Adopting a $2''$ radius[1] assures that all double entries are removed, which is especially important for the star count method (see next section). We therefore average the positions and fluxes of the stars located $< 2''$ from each other. We detect $\sim$ 70 000 distinct sources in I and J bands which are used to construct the extinction map (Section 3.1) and $\sim$ 20 000 sources detected in all 3 bands IJK_s.

3. Selection

3.1. Extinction map of the Cha II cloud

We construct an extinction map of the Cha II using the star count method developed by Cambrésy (1999). This method is based on the comparison of local stellar densities in the absorbed region and a nearby reference area assumed to be free of obscuration. DENIS provides stars detected in 2 infrared bands and 1 optical band. We first need to determine which band is the best one to apply this method. The K_s band allows to probe the dense cores of the cloud but the density contrast is too small to build an extinction map. We therefore use the I and J bands to construct the extinction map. By requiring that the stars be detected in both bands, we can eliminate spurious sources. But the simultaneous use of I and J bands introduces a bias which begins at $A_V = [(I-J)_{\rm limit} - (I-J)_{\rm average}]/[<A_I/A_V> - <A_J/A_V>]$. Fig. 2 shows that the average color of the stars $(I-J)_{\rm average} = 1$. Using the values of $<A_I/A_V>$and$<A_J/A_V>$ from Cardelli, Clayton, & Mathis (1989), we find that the bias begins at $A_V = (2-1)/(0.479-0.282)$=5. The bias can reach 2 magnitudes in the densest cores. As a result, less stars will be selected with a red color criterion.

We obtain $\sim$ 70 000 sources in I and J bands and use them to construct the extinction map. We use a wavelet transform algorithm to filter out the noise due the Poisson fluctuations in the star counts (Cambrésy, 1999). We take into account the decrease of stellar density with the latitude to calibrate the extinction as a function of galactic latitude. The slope of $A_V(b)$ is equal to 0 as suggested by the morphologic similarity with the ^{13}CO map of Mizuno et al. (1999). The absolute calibration for the extinction is obtained by assuming the extinction is 0 outside of the cloud. We use the extinction curve of Cardelli, Clayton, & Mathis (1989) to convert A_J into A_V ($A_J = 0.282 \times A_V$).

An alternative method to determine the extinction of individual stars consists of assuming an intrinsic color of stars and comparing this with the observed colors. However this method requires an assumption on the spectral types of the stars, of which we have no a priori information. The advantage of the star count method is that

[1] Note that these objects are located at the edges of the images, and therefore, their positional accuracy is worse than those located in the centre.

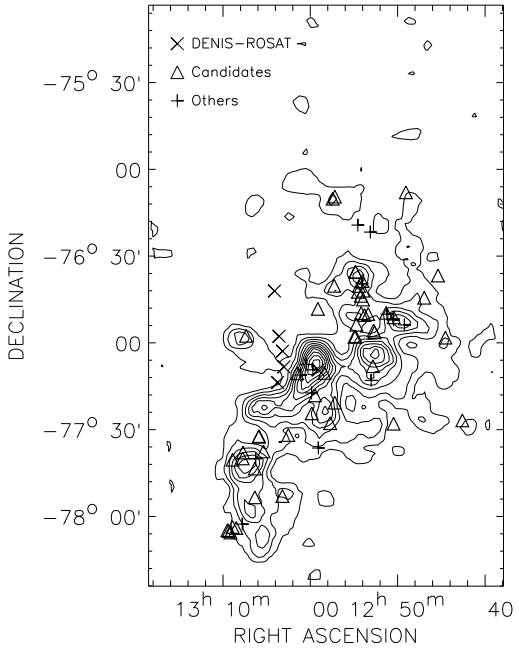

Fig. 1. Spatial distribution of low-mass TTS and/or young brown dwarf candidates (triangle signs) selected with $I - J \geq 2$ in the Cha II cloud. Six candidates cross-identified with ROSAT X-ray sources are presented. The plus signs are 15 bright candidates ($K_s \sim 8$). Contours indicate the extinction values beginning at $A_V = 1$ and spaced by 1 as derived from DENIS I and J counts. Coordinates are J2000.

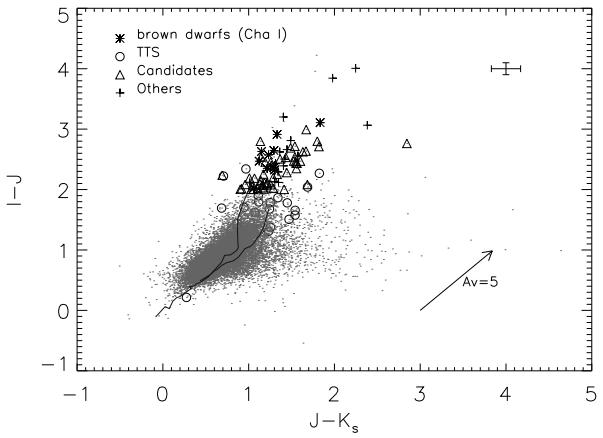

Fig. 2. $I - J/J - K_s$ color-color dereddened diagram for new DENIS selected low-mass TTS and/or young brown dwarf candidates (triangle signs) in Cha II cloud. The dots represent 20 000 stars detected in DENIS IJK_s bands in an area of 2.42° × 3.50° of the Cha II. The open dot signs represent known TTS in the Cha II. Eleven confirmed young brown dwarfs in Cha I cloud are also shown (Comerón et al., 2000). The plus signs are 15 bright candidates ($K_s \sim 8$). The main sequence, the giant branch and the extinction vector are also plotted. The representative error bar is shown in the upper right corner.

it provides an independent determination, at the expense of spatial resolution.

Fig. 1 shows the resulting extinction map of the Cha II with a spatial resolution of 2′. Note that Fig. 1 closely resembles the ^{13}CO map of Mizuno et al. (1999). The extinction values A_V range from 0 to 12. The statistical magnitude uncertainty due to the number of stars counted is approximately given by $1.3/\sqrt{(n+1)}$ (Rossano, 1980), where n is the number of stars counted per sampling element. Here, we have used $n = 20$ and the statistical uncertainty is ~ 0.30 magnitudes in A_J (~ 1.0 in A_V). We use this map to deredden all stars detected by DENIS in 3 bands IJK_s in this area.

3.2. Selection criterion

As shown by Delfosse (1997), the $I - J$ versus $J - K_s$ diagram is a powerful tool to separate low-mass TTS and young brown dwarfs from main sequence stars. Brown dwarfs and low-mass TTS have no hydrogen fusion when they are young. Thus, the nature of these objects is the same, and only their mass and/or temperature are different. This explains why they are both characterised by a deficit in I band because of the molecular absorption bands. Their youth is expressed by Hα emission and Li I absorption lines. But they are also characterised by features such as TiO and VO bands, and CaH, which allow the evaluation of the temperature and surface gravity. Kirkpatrick et al. (1991) have shown that these bands are very sensitive to the temperature of the environment in the M dwarfs. Because these features are located in the I-band, these objects have a strong I band deficit, while the J band flux is essentially photospheric in all these objects. Therefore, $I - J$ is a good estimator of the effective temperature in these objects. Thanks to the association of the optical I band to the infrared J and K_s bands in DENIS, we have derived a $I - J/J - K_s$ diagram (see Fig. 2) for ∼20 000 sources detected in three bands IJK_s. We only select sources after dereddening with $I - J \geq 2$ and spatially distributed in groups around the cloud cores. This provides a sample of 98 sources. After visual inspection on the DENIS images, we exclude 28 objects because they are located near the bleed-out trails of nearby saturated stars. We note that this selection criterion targets only young brown dwarfs and low-mass TTS. Massive TTS are characterised by their excess in K_s, thus in $J - K_s$ and $H - K_s$. Brown dwarfs and low-mass TTS have important $I - J$ but normal $J - K_s$.

Table 1 lists the remaining 70 low-mass young star candidates with their intrinsic photometric uncertainties, *i.e.* these do not include the uncertainties in the derived dereddening from the extinction map. Note that due to the bias (Sect. 3.1) introduced by I and J selection in the extinction map, less stars are selected in regions of high extinction. We identify 4 known TTS and 7 sources detected by IRAS within a 1′ radius in this sample. Four of

our candidates are also detected by ISO (P. Persi, private communication). Fig. 2 shows these candidates, and 11 spectroscopically confirmed brown dwarfs detected in the Cha I cloud (Comerón et al., 2000). We note that most of our candidates are located in the same region of the diagram as these known brown dwarfs.

3.3. Cross-identification with ROSAT sources

Weak line TTS are known as objects without a disk. Because of their relatively weak emission in the infrared (ascribed to the lack of dense surrounding matter), they can be more easily detected by their photospheric or coronal emission in X-ray surveys. Recently, Alcalá et al. (2000), using ROSAT PSPC observations, have detected 40 X-ray sources in the Cha II cloud, of which only 14 have been identified with previously known young stellar objects (IRAS sources, TTS). We cross-identified these 40 sources with DENIS IJK_s data, and identified these 14 known objects, plus 6 additional new WTTS candidates. We have also checked that these sources are located in the cloud (see Fig. 1).

4. Discussion and conclusion

4.1. Nature of the candidates

From the comparison of these objects with known TTS and young brown dwarfs (Fig. 3), we expect that most of our candidates are low-mass young stars such as young brown dwarfs or/and low-mass TTS. However, the true nature of the candidates is unambiguously confirmed only after a positive spectroscopic test such as the detection of the Hα emission line or/and the Li I absorption line, signatures of the youth of the stars. We will therefore observe these candidates spectroscopically. Hα emission is not unique to young low-mass objects. The detection of Li I from the photosphere can confirm the youth of the object (Martín et al., 1999). The detection of features such as CaH, TiI, NaI will allow the evaluation of the temperature and surface gravity (Kirkpatrick et al., 1991).

4.2. Evolutionary status

We use the evolutionary tracks for low-mass stars modeled by Baraffe et al. (1998) to estimate the mass and age of our low-mass star candidates. Fig. 3 shows the J versus $I-J$ color-magnitude diagram of our 70 candidates selected by $I-J \geq 2$ of which 4 are previously known TTS and six candidates cross-identified with ROSAT X-ray sources. We also plot the previously known TTS of the Cha II cloud identified with DENIS sources and the brown dwarfs of the Cha I detected and spectroscopically confirmed by Comerón et al. (2000). We used our extinction map (Fig. 1) to correct the reddening of all the objects shown in Fig. 3. We include the isochrones at 1 Myr, 10 Myr and 100 Myr from the Baraffe et al. (1998) model. The selection criterion of sources with $I-J \geq 2$ does not allow to distinguish low-mass candidates and stars located just behind the cloud. Their location in the color-magnitude diagram shows that they are separated by their luminosity. The location of low-mass candidates (except for the 15 bright candidates) in Fig. 3 suggests that they, indeed, have masses <0.2 $M_\odot$, and ages between 1 and 10 Myr. Although we selected these sources only with the $I-J \geq 2$ criterion, they are remarkably close to the evolutionary tracks of the model. This confirms that they probably are young brown dwarfs. Fifteen $I-J \geq 2$ candidates are bright sources ($K_s \sim 8$). Their infrared color excess $J-K_s$ is $\sim 1.5-2$ and $I-J \sim 2-4$. They do not appear to be field giants (expected to be uniformly distributed), but are located near the cloud cores in the extinction map. The number of giant field stars can be estimated using the so-called *Besançon model* (Robin & Creze, 1986). For the total Cha II area, the number of expected giant stars is about 400. A consequence of underestimating the extinction near the densest cores would be to select some giant stars near the cores. Only a spectroscopic follow-up can identify the nature of these objects.

4.3. Conclusion

We present the first extinction map of the Cha II cloud using the DENIS I and J band. We use this map to deredden all stars detected in 3 bands IJK_s, which allows to select low-mass young stars embedded in the cloud cores.

The location of our dereddened candidates selected with $I-J \geq 2$ in the color-magnitude diagram suggests that 51 of our candidates are probably low-mass TTS and/or brown dwarfs. However, a spectroscopic follow-up is necessary to confirm the true nature of these objects.

This selection is independent from the characteristics of the dark cloud and can thus be applied to all other star formation regions observed by DENIS in the South Hemisphere.

Acknowledgements. We are grateful to Dr. T. Montmerle for his helpful comments and to the anonymous referee for suggestions that improved this paper markedly. We warmly thank the members of the DENIS consortium whose work made these results possible. The DENIS project is partly funded by the European Commission through *SCIENCE* and *Human Capital and Mobility* grants. It is also supported in France by INSU, the Education Ministry and CNRS, in Germany by the Land of Baden–Würtenberg, in Spain by DGICYT, in Italy by CNR, in Autria by the Fonds zur Förderung der Wissenschaftlichen Forschung and Bundesministerium für Wissenschaft und Forschung.

References

Alcalá, J., et al. 2000, A&A, 355, 629
Baraffe, I., Chabrier, G., Allard, F., & Hauschildt, P. 1998, A&A, 337, 403 1997, ApJ, 491, 856
Cambrésy, L., et al. 1998, A&A, 338, 977
Cambrésy, L. 1999, A&A, 345, 965
Cardelli, J., Clayton, G., & Mathis, J. 1989, ApJ, 345, 245

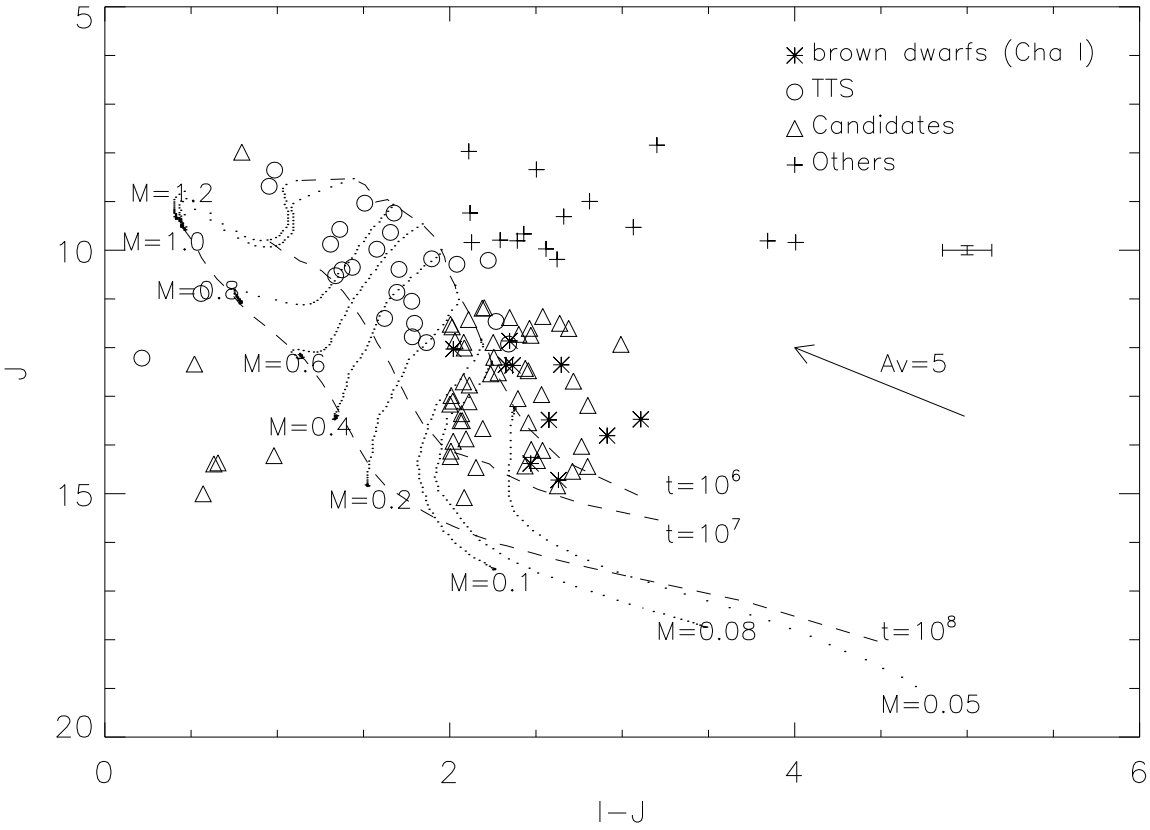

Fig. 3. J vs. $I-J$ magnitude-color diagram for the Cha II dark cloud. Selected low-mass TTS and/or young brown dwarf candidates are indicated with triangles. We show the 1 Myr, 10 Myr and 100 Myr isochrones (dashed lines) from the Baraffe et al. (1998) model. Open circles denote known TTS of the Cha II. Star symbols are brown dwarfs detected and spectroscopically confirmed by Comerón et al. (2000). The plus signs are 15 bright candidates also selected with $I-J \geq 2$. The representative error bar is given.

Comerón, F., Neuhäuser, R., & Kaas, A. 2000, A&A, 359, 269

Delfosse, X. 1997, thesis Université de Grenoble

Deutsch, E. W. 1999, AJ, 118, 1882

Epchtein, N., et al. 1997, The Messenger, 87, 27

Gómez, M. & Kenyon, S. 2001, AJ, 121, 974

Hartigan, P. 1993, AJ, 105, 1511

Kirkpatrick, J., Henry, T., & McCarthy, D. 1991, ApJS, 77, 417

Larson, K., Whittet, D., Prusti, T., & Chiar, J. 1998, A&A, 337, 465

Martín, E., Basri, G., & Zapatero Osorio, M. 1999, AJ, 118, 1005

Méra, D., Chabrier, G., & Baraffe, I. 1996, ApJ, 459, L87

Mizuno, A., et al. 1999, PASJ, 51, 859

Monet, D., et al. 1998, USNO-SA2.0, (U.S. Naval Observatory, Washington DC)

Montmerle, T., Grosso, N., Tsuboi, Y., & Koyama, K. 2000, ApJ, 532, 1097

Neuhäuser, R. & Comerón, F. 1999, A&A, 350, 612

Oasa, Y., Tamura, M., & Sugitani, K. 1999, ApJ, 526, 336

Olmi, L. 1994, A&A, 288, 591

Persi, P., et al. 2000, A&A, 357, 219

Prusti, T., Whittet, D., Assendorp, R., & Wesselius, P. 1992, A&A, 260, 151

Robin, A. & Crézé, M. 1986, A&A, 157, 71

Rossano, G. 1980, AJ, 85, 1218

Schwartz, R. 1977, ApJS, 35, 161

Tinney, C. 1993, ApJ, 414, 279

Vilas-Boas, J., Myers, P., & Fuller, G. 1994, ApJ, 433, 96

Whittet, D., et al. 1997, A&A, 327, 1194

Yamauchi, S., Hamaguchi, K., Koyama, K., & Murakami, H. 1998, PASJ,50, 465

Table 1. Photometric data of the selected candidates ($I - J \geq 2$)

ID[a]	α(J2000)	δ(J2000)	I^b	J^b	K_s^b	A_V	Ref.[c]
C1	12 43 53.1	−77 29 44.6	16.97±0.12	14.67±0.12	13.41±0.19	0.7	
C2	12 46 08.7	−77 01 02.7	17.77±0.44	14.75±0.13	13.43±0.17	1.1	
C3	12 47 11.7	−76 39 29.8	16.49±0.16	14.34±0.11	13.31±0.17	0.7	
C4	12 48 28.5	−76 47 11.6	17.31±0.20	14.53±0.11	12.74±0.12	1.5	1
C5	12 50 22.2	−76 56 37.9	16.51±0.08	11.49±0.06	8.51±0.06	6.0	
C6	12 50 39.7	−76 10 39.1	17.32±0.12	14.70±0.12	12.98±0.14	1.0	1
C7	12 51 10.5	−77 30 54.0	17.26±0.03	15.14±0.04	13.42±0.08	0.2	
C8	12 51 28.3	−76 54 00.3	17.67±0.15	14.56±0.12	12.44±0.12	5.6	5
C9	12 51 29.0	−76 54 55.5	14.86±0.04	11.29±0.06	9.01±0.06	5.8	
C10	12 51 30.5	−76 54 37.7	14.42±0.04	10.54±0.05	8.13±0.06	5.5	
C11	12 52 11.0	−76 52 53.3	15.73±0.06	10.95±0.05	8.04±0.07	3.9	
C12	12 52 15.5	−76 52 25.6	17.51±0.14	14.64±0.12	13.05±0.16	3.5	
C13	12 52 30.6	−77 15 13.1	12.21±0.02	9.10±0.05	7.25±0.08	4.1	1,2
C14	12 53 23.4	−76 59 11.3	17.81±0.17	14.90±0.14	13.19±0.18	2.1	
C15	12 53 29.7	−76 58 34.9	16.88±0.10	14.41±0.12	12.96±0.16	1.9	
C16	12 53 29.8	−77 10 56.8	16.74±0.10	13.43±0.09	11.41±0.10	6.6	5
C17	12 53 38.9	−77 15 53.2	15.25±0.05	11.63±0.07	9.41±0.08	5.1	1
C18	12 54 00.2	−76 24 25.1	11.52±0.02	8.12±0.05	6.55±0.09	1.0	
C19	12 54 05.2	−76 52 51.3	16.13±0.07	13.50±0.09	11.88±0.11	2.6	
C20	12 54 27.1	−76 53 14.3	16.86±0.11	14.26±0.11	12.65±0.14	2.7	
C21	12 54 36.2	−76 44 45.2	17.99±0.18	14.90±0.14	13.28±0.19	2.8	
C22	12 54 37.3	−76 47 50.6	16.37±0.09	13.87±0.10	12.40±0.11	2.5	1
C23	12 54 42.6	−76 41 25.8	17.06±0.12	13.73±0.09	11.79±0.10	4.4	
C24	12 54 45.2	−76 42 19.5	14.11±0.04	10.99±0.05	8.93±0.07	4.2	
C25	12 54 47.4	−76 52 32.5	16.89±0.11	14.22±0.11	12.54±0.12	3.0	
C26	12 54 50.8	−76 46 32.4	16.80±0.10	14.23±0.11	12.74±0.14	2.6	5
C27	12 55 03.3	−76 43 07.8	15.21±0.05	12.26±0.07	10.33±0.07	3.8	
C28	12 55 08.7	−76 45 10.4	16.04±0.07	13.44±0.08	11.74±0.09	2.6	
C29	12 55 14.4	−76 22 00.5	12.41±0.03	10.10±0.05	8.64±0.06	0.9	
C30	12 55 15.7	−76 56 33.1	15.45±0.06	12.27±0.07	10.14±0.07	2.7	1
C31	12 55 20.7	−77 00 35.9	15.18±0.05	12.11±0.07	10.13±0.07	2.7	
C32	12 55 24.0	−76 38 17.6	17.44±0.15	13.88±0.10	11.63±0.09	4.2	
C33	12 55 25.7	−77 00 46.5	15.31±0.05	12.58±0.07	10.84±0.08	2.4	
C34	12 55 25.7	−76 38 10.9	17.47±0.14	14.24±0.11	12.23±0.11	4.2	
C35	12 57 25.9	−77 23 35.2	17.04±0.13	14.18±0.10	12.33±0.11	3.8	
C36	12 57 29.3	−76 12 06.5	15.00±0.04	12.49±0.07	10.92±0.08	2.1	
C37	12 57 31.5	−76 43 04.4	15.58±0.06	12.55±0.07	10.47±0.07	2.9	1
C38	12 57 41.6	−76 12 51.2	15.96±0.07	13.07±0.08	11.13±0.08	2.3	
C39	12 57 54.5	−77 30 43.5	15.75±0.06	12.73±0.07	10.73±0.07	4.6	

ID[a]	α(J2000)	δ(J2000)	I^b	J^b	K_s^b	A_V	Ref.[c]
C40	12 58 31.4	−77 13 16.4	17.73±0.17	14.00±0.10	11.49±0.08	8.8	
C41	12 59 09.8	−76 51 03.5	16.82±0.10	14.04±0.10	11.19±0.09	0.1	1
C42	12 59 10.7	−77 39 19.1	12.91±0.02	9.86±0.05	8.08±0.06	2.0	
C43	12 59 30.3	−77 21 04.6	17.27±0.12	13.97±0.09	11.66±0.09	5.2	
C44*	12 59 42.8	−77 12 12.8	15.68±0.06	11.27±0.05	8.29±0.05	11.7	
C45	12 59 51.8	−77 27 18.9	16.20±0.08	12.86±0.07	10.56±0.07	4.5	
C46*	12 59 52.1	−77 20 15.0	14.30±0.03	10.97±0.06	8.59±0.06	6.2	
C47*	13 00 24.1	−77 10 22.4	17.18±0.12	12.71±0.07	9.51±0.06	9.7	
C48*	13 00 59.3	−77 14 02.7	16.40±0.08	11.77±0.09	8.05±0.08	7.9	
C49*	13 01 21.4	−77 13 25.2	17.62±0.15	13.52±0.11	10.90±0.10	5.6	
C50	13 02 22.9	−77 34 49.5	15.42±0.05	12.77±0.10	11.26±0.11	2.0	
C51	13 03 09.1	−77 55 59.5	14.46±0.04	11.83±0.07	10.38±0.08	2.3	
C52	13 05 05.1	−77 40 31.3	17.34±0.14	13.98±0.10	11.71±0.10	2.8	
C53	13 05 08.6	−77 33 42.5	14.68±0.04	12.02±0.06	9.87±0.07	2.0	3
C54	13 05 30.9	−77 35 11.9	17.10±0.11	14.75±0.12	13.03±0.17	1.8	
C55	13 05 32.7	−77 35 26.2	14.60±0.04	11.89±0.06	10.03±0.06	1.8	
C56	13 05 57.1	−77 43 00.5	13.74±0.03	10.05±0.04	7.61±0.05	6.0	
C57	13 06 04.8	−77 46 28.3	16.75±0.09	13.54±0.08	11.38±0.08	6.0	
C58	13 06 11.1	−77 56 26.4	17.64±0.15	14.92±0.13	13.04±0.17	3.5	
C59	13 06 30.8	−77 00 24.0	15.96±0.07	12.59±0.07	10.52±0.07	3.5	
C60	13 06 56.5	−77 23 09.5	13.59±0.03	10.89±0.05	9.78±0.06	2.4	4
C61	13 06 57.4	−77 23 41.5	13.56±0.03	11.01±0.05	8.90±0.06	2.6	1,4
C62	13 07 18.1	−77 40 53.0	16.07±0.07	13.17±0.07	11.52±0.08	4.1	
C63	13 07 21.4	−77 42 55.6	17.81±0.20	14.69±0.12	12.64±0.12	5.6	5
C64	13 07 41.2	−78 05 43.3	13.17±0.03	10.38±0.05	8.63±0.06	2.0	
C65	13 08 22.8	−78 07 04.6	14.95±0.04	12.21±0.06	10.66±0.07	1.7	
C66	13 08 27.2	−77 43 23.3	16.53±0.09	13.57±0.08	12.26±0.10	3.7	
C67	13 08 46.8	−78 06 44.5	16.50±0.09	13.84±0.09	12.40±0.12	1.0	1
C68	13 09 02.4	−78 08 38.6	15.95±0.07	13.23±0.07	11.64±0.08	0.9	
C69	13 09 14.6	−78 08 06.3	17.62±0.18	14.75±0.12	12.81±0.15	0.8	
C70	13 09 21.6	−78 07 47.8	17.81±0.20	15.04±0.14	13.29±0.19	0.7	
X1	12 59 10.1	−77 12 13.7	14.29±0.03	11.23±0.06	9.19±0.06	11.5	
X2	13 02 42.3	−77 11 11.1	15.68±0.03	14.75±0.09	13.50±0.13	1.4	
X3	13 02 49.2	−77 05 44.6	15.31±0.05	14.28±0.13	13.33±0.19	0.2	
X4	13 03 09.0	−77 00 32.8	13.18±0.03	12.53±0.08	11.96±0.11	0.7	
X5	13 03 23.9	−77 16 37.1	15.45±0.05	14.64±0.12	13.46±0.22	0.9	
X6	13 03 30.5	−76 44 51.4	15.57±0.05	15.00±0.14	13.50±0.22	0.0	

[a] C=Colour selected candidate; X=X-ray selected candidate; *=object detected by ISO (P. Persi, private communication)

[b] Observed magnitudes. The intrinsic photometric uncertainty is given for each star.

[c] REFERENCES: (1): IRAS; (2):Larson et al. (1998); (3):Hartigan (1993); (4):Schwartz (1977); (5): Vilas-Boas et al. (1994)